

APRIL 2020

RubberWorld

years
131

THE TECHNICAL SERVICE MAGAZINE FOR THE RUBBER INDUSTRY VOLUME 262, No.1

**Elastomer sealing performance
in hydrogen fuel cells**

**Fuel aging studies
of AEM compounds**


**Therban HT: Polyamide reinforced HNBR
with improved high temperature properties**

**Optimizing rubber products for automotive
via characterization of compounds and computer modeling**

www.rubberworld.com

**Rubber
Division**

American Chemical Society
ACS Events, page 52

 @rubberworld

Contents

Vol. 262, No. 1 April 2020

FEATURES

16 Elastomer sealing performance in hydrogen fuel cells

by Kevin Kulbaba and Jacob Rawski, Arlanxeo; Edward Norton, Cancarb; and Rick Ziebell, R.D. Abbott. Careful selection of an elastomer and filler system can achieve low permeation rates in flexible hoses and seals.

28 Fuel aging studies of AEM compounds

by Edward McBride, DuPont. AEM samples were aged in fuel using the standard liquid phase testing, while other samples were aged in the vapor phase above the fuel, and AEM compounds aged in the vapor phase performed much better.

36 Therban HT: Polyamide reinforced HNBR with improved high temperature properties

by Marjan Hemstede-van Urk, Pete Spanos, Jelena Dodevski, Andreas Kaiser and Susanna Lieber, Arlanxeo. Therban HT is a novel technology to improve the heat resistance of HNBR compounds with the use of plastic reinforcement, while maintaining media resistance.



Cover photo: Courtesy of AGC Chemicals Americas

44 Optimizing rubber products for the automotive industry via characterization of compounds and rubber product computer modeling

by Ben Chouchaoui, Windsor Industrial Development Laboratory. Tests related to rubber necessary to building quasi-static rubber product models for the automotive industry are described.

DEPARTMENTS

4 Editorial

7 Business Briefs

10 Market Focus

12 Oil, Gas & Energy

14 Patent News

50 Meetings

56 Suppliers Showcase

61 People in the News

Elastomer sealing performance in hydrogen fuel cells

by Kevin Kulbaba and Jacob Rawski, Arlanxco; Edward Norton, Cancarb; and Rick Ziebell, R.D. Abbott

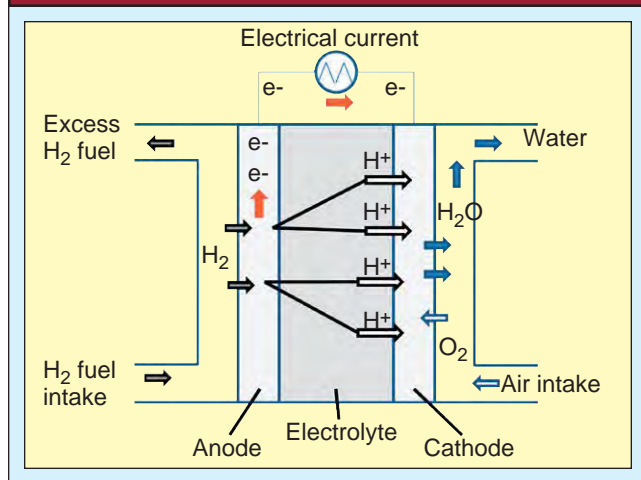
Hydrogen fuel cells are currently in operation over a wide range of applications, classified primarily by the kind of electrolyte they employ. These include molten carbonate fuel cells (MCFC), solid oxide fuel cells (SOFC), phosphoric acid fuel cells (PAFC), direct methanol fuel cells (DMFC), and low and high temperature polymer electrolyte membrane (PEM) fuel cells. Only the last two are adaptable to automobiles due to DOT restrictions for safety.

Fuel cell types and limitations for onboard automotive use include:

- MCFCs operate at extremely high temperatures of 650°C. They are not used in automotive. They are used industrially in steam reforming.
- SOFCs create waste heat at a temperature level of more than 600°C. They are not used in automotive. They are used industrially in steam reforming.
- PAFCs operate at around 200°C. They are not used in automotive. They were used in Apollo missions by NASA.
- DMFCs operate at pressures ranging from near ambient to about 6 atm (atmospheric pressure), and at temperatures between 50°C and 120°C. They represent older technology. They require hot pressurized methanol.
- PEMs operate at pressures ranging from near ambient to about 700 kPa (7 atm), and at temperatures between 50°C and 90°C.

From an applicability point of view, PEM is a breakthrough technology in fuel cell design for automotive. As an example, the Toyota Mirai FCV (fuel cell vehicle) (ref. 1) is the showcase of this technology. It uses a low temperature polymer electrolyte membrane (PEM) fuel cell stack, and is regarded as a major improvement over fuel cells of the past. Figure 1 shows a general schematic of how a PEM fuel cell works.

Figure 1 - schematic of a PEM fuel cell



On board hydrogen delivery is by way of equipment carrying the gas through gaskets and hoses (figure 2). The study is relevant to applications in storage, hydrogen supply and the PEM system assembly, as well, since the hydrogen gas fuel is stored on board and delivered through rubber containing gaskets and hoses. Therefore, low permeation of hydrogen through these sealing elements is needed for better fuel cell performance (or reduced loss of fuel). At a 90°C upper operating temperatures and 700 kPa atmospheric pressure, the study will examine low permeation compounds that can handle moderate heat.

Background

Previous work

In review of technical content, this article extends upon a study by M.W. Fitch et al. (ref. 2). The report characterized many polymers by the ability to allow different gases, including hydrogen gas, to permeate. Fitch detailed the mechanism that controls permeation of gasses through a membrane. Starting with Fick's law, the mechanism is both a function of diffusion and sorption of the gas molecules in the polymer matrix. Graham (ref. 3) postulated that gas molecules first dissolve into a solid membrane and then transport through it by diffusion. Wroblewski (ref. 4) found that steady state diffusion is achieved by a driving pressure differential across the membrane. Fick's laws of diffusion can then be solved for a constant pressure differential, showing that permeation is the product of the solubility and diffusion coefficients. Several key permeation factors were outlined by Fitch. Selected summary permeation data are provided in table 1 for various gases through rubber membranes tested at 35°C and 2 to 18 atmosphere pressures (actual pressures not specified).

Fitch found that butyl rubber's (BIIR) actual permeation resistance fell below Fick's law predictions. This unique phenomenon is the main reason why butyl rubber is chosen as a gas barrier

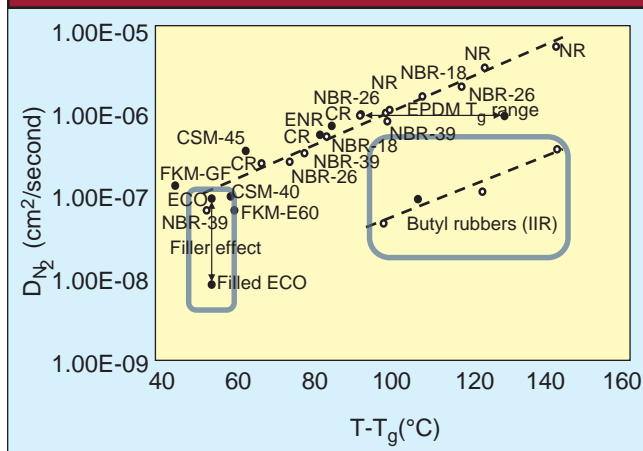
Figure 2 - hydrogen fuel cell vehicle H₂ storage and delivery system



Table 1 - permeation data for selected elastomers with different gases (ref. 2)

Selected elastomers:	He	H ₂	D ₂	O ₂	N ₂
Butyl rubbers (IIR)	14.1 - 16.4	11.7 - 13.8	11.0 - 11.3	2.50 - 2.80	0.69 - 0.76
Chlorosulfonated polyethylenes (CSM)	8.8 - 11.5	11.0 - 15.6	10.2 - 14.9	2.37 - 4.20	0.63 - 1.28
Fluoroelastomers (FKM)	30.5 - 43.9	10.6 - 21.8	10.0 - 20.9	2.28 - 4.20	0.85 - 2.13
Epichlorohydrin (ECO)	5.5	8.9	8.8	1.05	0.44
Ethylene propylene diene (EPDM)	33.6	49.4	45.8	21.14	8.33
Polychloroprenes (CR)	20	27.6	26.7	8.83	2.97

Permeation data presented in barrer; 1 barrer = 10⁻¹⁰ (cc[STP]cm)/(cm²[cm Hg]s); error ±10%.

Figure 3 - diffusion coefficients relative to glass transition temperature (ref. 2)

material for many applications, with most commercially available butyl rubber polymers being used for tire inner liners. Fitch writes: "It seems the reason for (butyl's) enhanced permeation resistance is that the packing of the chains is still tight enough to provide little free volume to promote gas dissolution." We believe what Fitch is implying here is that free volume can limit permeation, where the lower the free volume, the greater the permeation resistance. It was also found that certain fillers can reduce the permeation rates, causing the composite material to fall outside the predicted Fick's law factors. Fitch noted that filler can decrease the diffusion coefficients by an order of magnitude.

In figure 3, diffusion coefficients from Fitch and Amerongen (ref. 5) are graphed relative to the specific polymer glass transition temperature. Here it is shown that the diffusion coefficients (D) of various elastomers (NBR, NR, ECO, FKM, etc.) with a wide range of T_g values can be plotted on a single line, apart from butyl rubber, which falls well below the line. Amerongen also noted that in an elastomer, the diffusional path can be made longer and significantly more tortuous by providing an impermeable obstacle to diffusion with addition of idealized filler structures to the rubber compound. In figure 3, the blue boxes illustrate butyl's unique performance and the additional effect a plate-like filler can have on diffusion in an elastomeric compound.

From both Fitch and Amerongen, the two most valuable factors for creating low permeation rates in a rubber compound are the selection of base polymer itself and a filler system that will create a tortuous path to gas diffusion. Additional factors which may have an impact on diffusion through a polymer network

include the free volume and mobility of the polymer chains, which can be influenced by crosslinking, molecular weight, degree of unsaturation and the nature of the substituents along the polymer main chain (ref. 6).

Experimental

Problem statement

The on-board PEM system operates under 7 atmospheric pressure; but with the higher the operating pressure, the more electrical power the fuel cell generates. What is true for the membrane that creates the power is also true for the on-board hydrogen supply system. However, hoses and seals must hold back the hydrogen gas at 7 atmospheric pressure, and permeation loss is a loss of expensive hydrogen fuel, which lowers the overall efficiency of the vehicle; and not to mention the even more important concerns regarding safety due to the potential of explosion from ignition of escaped hydrogen gas.

Materials

This study will primarily examine X_Butyl BB 2030 (BIIR) with tortured path resistance derived from the addition of Thermax N-990 as a ratio to Mistrion HAR talc and total filler level. Figure 4 shows the structure of the polymer.

Plate-like fillers are well known to improve the permeation resistance of elastomers by increasing the tortured path for gas molecules to transmit through the material. High aspect ratio (HAR) talc is a common filler employed in compounding elastomer materials which has such a plate-like structure (figure 5). Mineral deposits of this type can remain stacked in a connected

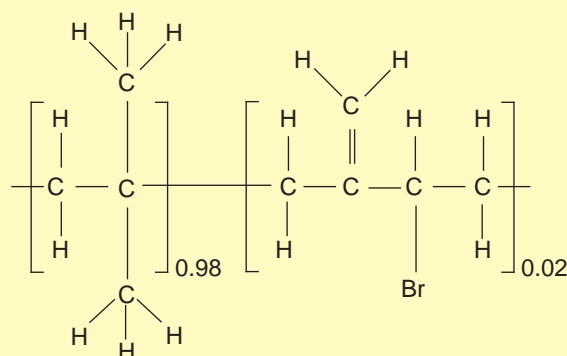
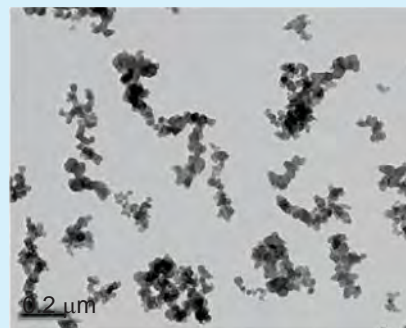
Figure 4 - bromobutyl rubber (BIIR) chemical structure

Figure 5 - fillers for dispersion, tortured path resistance and mechanical structure



Furnace black (N-330)

layering of plates during standard mixing processes, creating dispersion difficulties. In these densely packed structures, the plates are not adequately dispersed and are less effective at providing tortured path resistance to diffusion.

The tortured path resistance can be further enhanced by addition of fillers that aid in the separation of Mistrion HAR talc platelets, such as a thermal carbon black (N-990). Thermax N-990 has large and small particles, averaging 280 nm in diameter, and there is a wide distribution of particle sizes that are somewhat spherical in shape (figure 5). A third filler component (a furnace black N-330) was used, due to the increased structure to provide better reinforcement to the compound and enhance the resulting tensile properties. In contrast, Thermax N-990 has a low structure, with only a few primary particles per aggregate. Systems of this type provide a much more closely packed arrangement of fillers and serve to maintain the improved dispersion of the Mistrion HAR talc layers within the elastomer matrix, as illustrated in figure 6.

Carbon black typically has a crystalline nanostructure con-

sisting of graphitic layers. Figure 7 shows the highly ordered surface layers of an N-990 particle, which become more ordered as the primary particle size increases. The edges of these layers have dangling bonds, unsatisfied valences on the carbon atoms (defects), which can act as reactive sites. Smaller particle size carbon blacks, which have not been treated or graphitized, will have higher surface activity because they have a higher degree of disorder, a rougher surface and more exposed edges (ref. 7).

The surface chemistry of N-990 consists of relatively low concentrations of hydroxyl, carbonyl and carboxyl functional groups (as well as phenol, lactone, quinone, etc.) as compared to furnace blacks. These functional groups will influence how the surface will interact with different molecules. For example, oxidizing these structures increases the number of oxygen functional groups, and will generally increase the hydrophilic sorption of water.

The spacing between overlapping graphitic layers in N-990 particles is like that found in graphite, with a relatively small plane-to-plane gap of only approximately 3.4 Å (ref. 8). Consider-

Compound formulations		phr ^a																						
X_Butyl BB 2030	100	→					100	→					100	→					100	→				
Mistron HAR talc	0		20		40	60	0		16		32	48	1		12		24	36	0		8		16	24
Thermax N-990	100		80		60	40	80		64		48	32	60		48		36	24	40		32		24	16
N-330	35	→					35	→					35	→					35	→				
Paraffinic oil	10		11.7		13.3	15	7.5		8.8		10.2	11.5	5		6		7	8	2.5		3.2		3.8	4.5
N-990 ratio	1		.8		.6	.4	1		.8		.6	.4	1		.8		.6	.4	1		.8		.6	.4
Total filler phr	135	→					115	→					95	→					75	→				
Sulfur cure:		phr ^a																						
Stearic acid	1																							
Zinc oxide	3																							
MBTS accelerator	1.3																							
Sulfur	0.5																							
Resin cure:		phr ^a																						
Stearic acid	1																							
Zinc oxide	3																							
Resin	1.5																							

Mixing procedure:

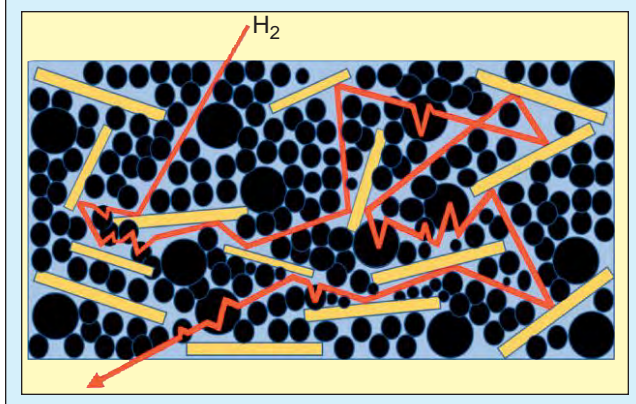
Stage 1: Internal mixer,
60 rpm
0 seconds - add polymer
60 seconds - add filler
105°C - add oil
115°C - sweep
135°C - drop batch

Stage 2: Internal laboratory mixer, 50 rpm
0 seconds - add 4/5 of stage 1
70°C - add curatives and 1/5 stage 1
115°C - drop batch

Stage 3: Laboratory mill, drive ratio 1:1.4
Compounds were refined with six 3/4
cuts and six endwise passes on a
6 x 12 inch mill at 20 rpm at 50°C

^a Ingredient amounts given relative to the amount of rubber, units of phr (parts per hundred of rubber)

Figure 6 - tortured path diffusion resistance with Thermax N-990 and Mistrion HAR talc



ing tortured path resistance, N-990 has an idealized plate-like graphitic structure that allows small gaseous atoms to diffuse into the interlayer space and become temporarily trapped. Gas entrapment and sequestering of the gas molecules decrease the gas molecules' diffusion rate through the matrix by contributing to the tortured path distance. The smaller and more mobile the gas molecule, the more apparent the interactions between the gas molecule and the graphitic layers become. In this way, the carbon black may be capable of affecting the permeation pathway of small molecules, such as hydrogen, compared to larger gas molecules, such as oxygen. Furthermore, gas molecules that can ionize may become sequestered within the graphitic structure, and then be reformed as a different molecule. A. Jelea et al. found that hydrogen gas can interact with oxygen between graphitic planes to form epoxide-like structures. Hydrogen gas sequestered in this manner can readily recombine to form water molecules. The interactions of the hydrogen ions with graphite planes are of the van der Waals type, and occur with no activation barrier (ref. 9).

Experimental design

Table 2 lists the complete four-by-four compound design, which is cured using either a standard sulfur cure or a resin cure system. Compounds were designed to have similar hardness (iso-hardness) to allow for a better comparison of the physical properties and permeation resistance between all compounds in the study. Each compound is designed to have fixed ratios of Thermax N-990 at increasing total filler loadings. Permeation properties of compounds are known to be greatly improved with higher filler loading, or with reduced oil contents, and these effects should be considered. As mentioned previously, a reinforce-

Figure 7 - high resolution TEM image of N-990 nanostructure

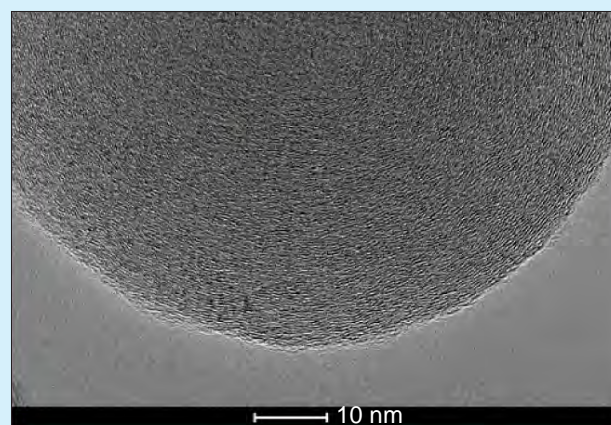
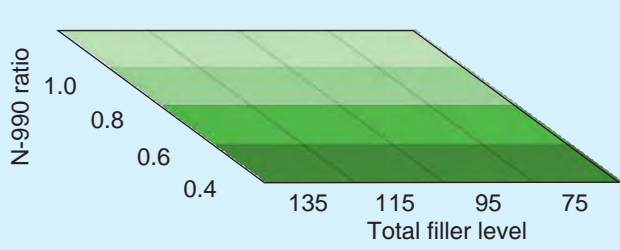


Figure 8 - experimental design space



ing carbon black (N-330) was added to all compounds at a constant loading to improve physical properties.

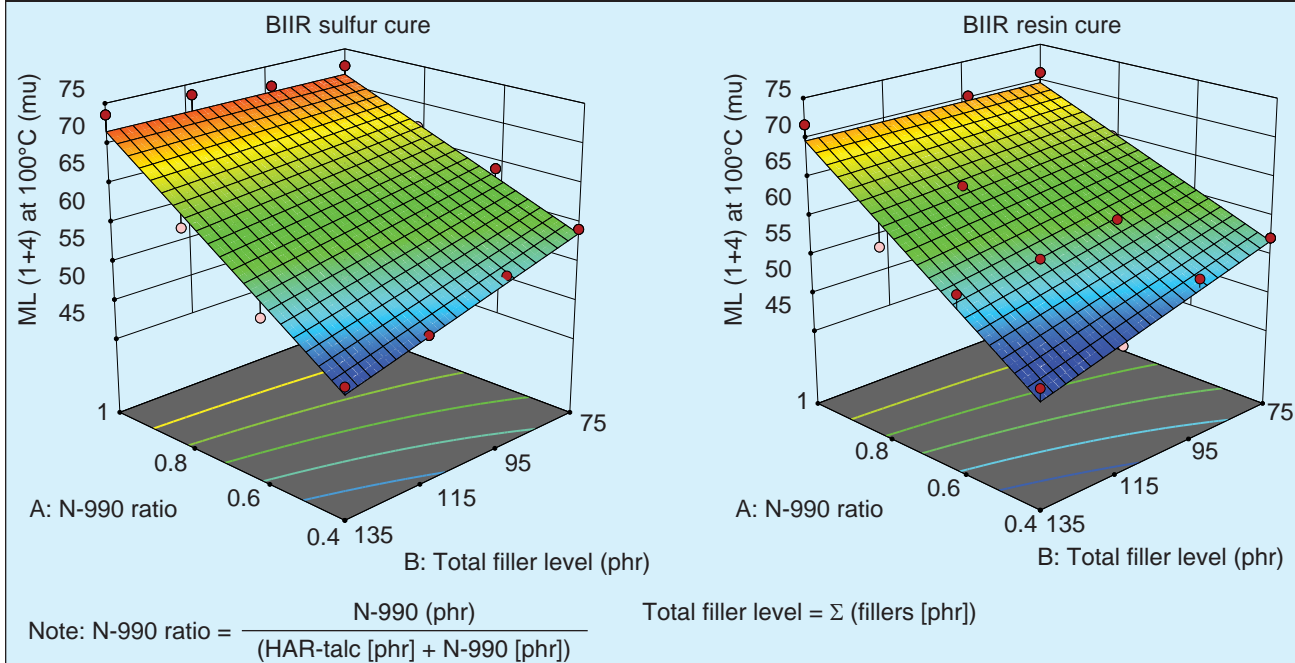
X_Butyl BB 2030 (BIIR) was chosen due to its inherently low permeation properties, as outlined above. A standard sulfur cure system provides a baseline for the permeation testing and to reach the desired physical requirements for a hose or seal application. A resin cure system provides improved heat and aging resistance (a more thermally stable network) and reduced compression set properties. In terms of permeation resistance, the thermoplastic nature of the resin may also have influence on diffusion of certain gases. Target physical properties include ultimate tensile values of >8 MPa, compression set values of <25% at 100°C for 70 hours, and lowest possible permeation rates for O₂ and H₂ gases. All compounds were mixed using a laboratory scale Brabender internal mixer equipped with tangential Banbury rotors with an internal mixing volume of 375 ml. Compounds were mixed using a three-stage mixing procedure, outlined in table 2, with a fill factor of 0.73 and an initial start temperature of 60°C. The compound mixing order for each curative type was randomized to avoid bias.

The experimental design aims to evaluate X_Butyl rubber compounds with different tortured path resistance filler systems, and to separately consider the impact of the two cure systems (see table 3 for suppliers). The experimental design space (figure 8) is arranged in a four-by-four for each BIIR cure system, requiring a total of 32 compounds. In mixture designs, it is often necessary to tie concentration level changes of individual ingredients to ratios and totals. In this manner, the change of one ingredient can be studied as an effect of the total change in all in-

Table 3 - polymers and fillers used in this study

Material	Supplier	Grade
Bromobutyl rubber (BIIR)	Arlanxeo	X_Butyl BB 2030
Thermal carbon black	Cancarb	Thermax N-990
Furnace carbon black	Birla Carbon	N-330
High aspect ratio (HAR) talc	Imerys	Mistrion HAR talc

Figure 9 - Mooney viscosity at 100°C response surface models (ASTM D1646)



gradient levels. This method of comparison creates a smooth proportional design space with all ingredients held to orthogonal constraints. N-990 ratio is the filler loading in phr of N-990/[N-990 + HAR talc], and the total filler level is the sum of N-990, HAR talc and N-330. In order to target similar grades throughout the experimental design space, an iso-hardness constraint was set at 68 ± 5 durometer A. To satisfy this constraint, the free oil content was adjusted as the N-990 ratio and total filler level changed.

Results

Processing properties

Viscosity, $\tan \delta$ and scorch time were used to assess processing performance. Lower viscosity in general allows for higher throughput in extrusion operations, and for better filling of cavities during injection molding operations. Compounds with higher $\tan \delta$ values are typically better for processing, as they will flow and form more readily. Low $\tan \delta$ values often reflect a compound

Figure 10 - storage modulus (G') response surface models, 1.0% strain amplitude, 0.1 Hz and 60°C (ASTM D6204)

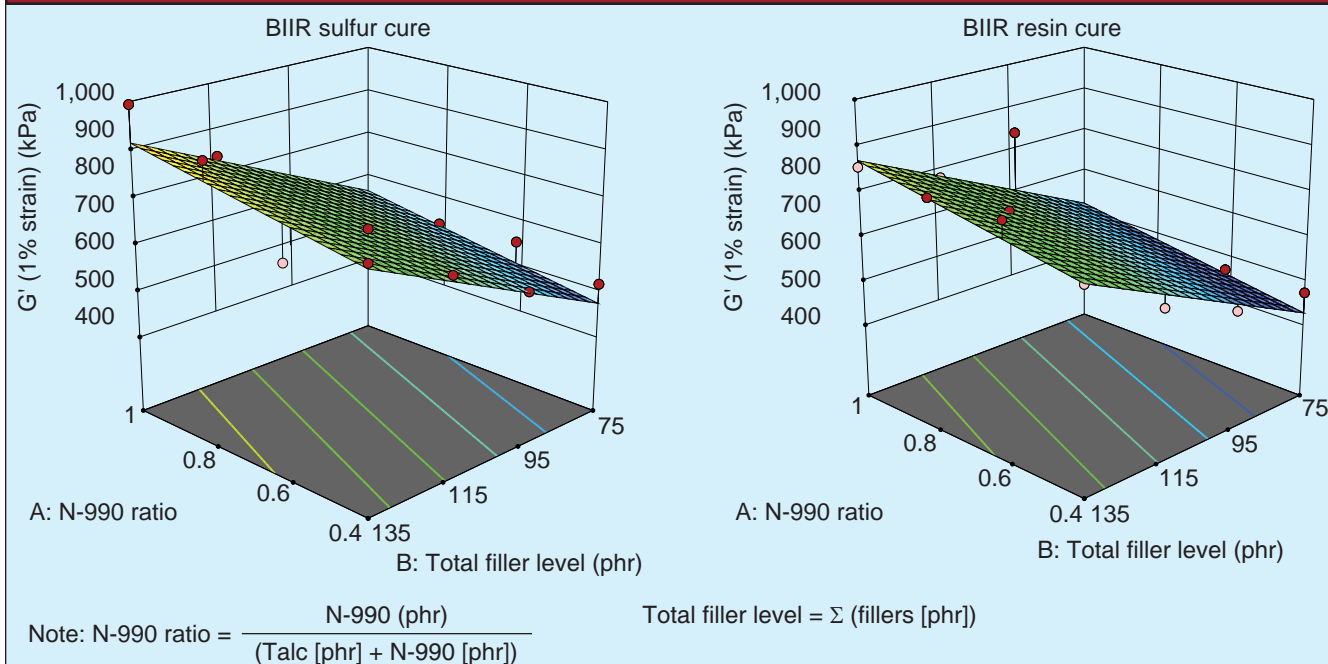
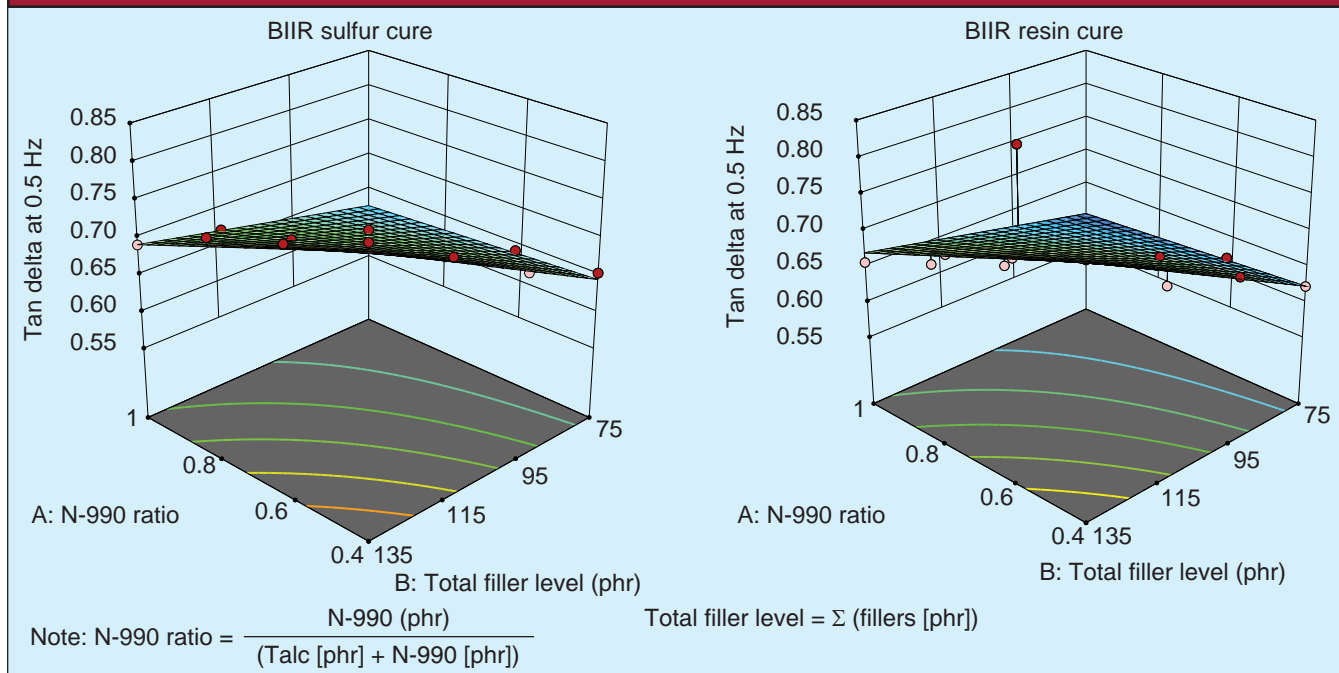


Figure 11 - $\tan \delta$ response surface models for compounds at 7% strain amplitude, 0.5 Hz and 100°C (ASTM D6204)



that is nervy and difficult to work with. Occasionally, compounds with higher $\tan \delta$ values may have issues with scorch (premature curing) if processing conditions create significant viscous heating. Longer scorch times allow for larger processing windows, and a given process will require a certain amount of scorch safety in order to avoid generating large amounts of scrap in the form of poorly formed rubber articles, including seals or hoses.

The results were analyzed, modeled, and all plots were

graphed using Design Expert Software version 11, developed and sold by Stat-Ease Inc. Figure 9 shows the response surface models for the compound Mooney viscosity at 100°C. Values ranged from 50 to 74 mu for the compounds, with the viscosity increasing with increasing N-990 ratio, and decreasing total filler content. This effect can be considered complex in that the oil content varied to achieve iso-hardness. The oil content generally increased with increasing filler loading, and that is a major contributor to the

Figure 12 - ts2 response surface models for compounds, MDR at 1° arc and 160°C (ASTM D5289)

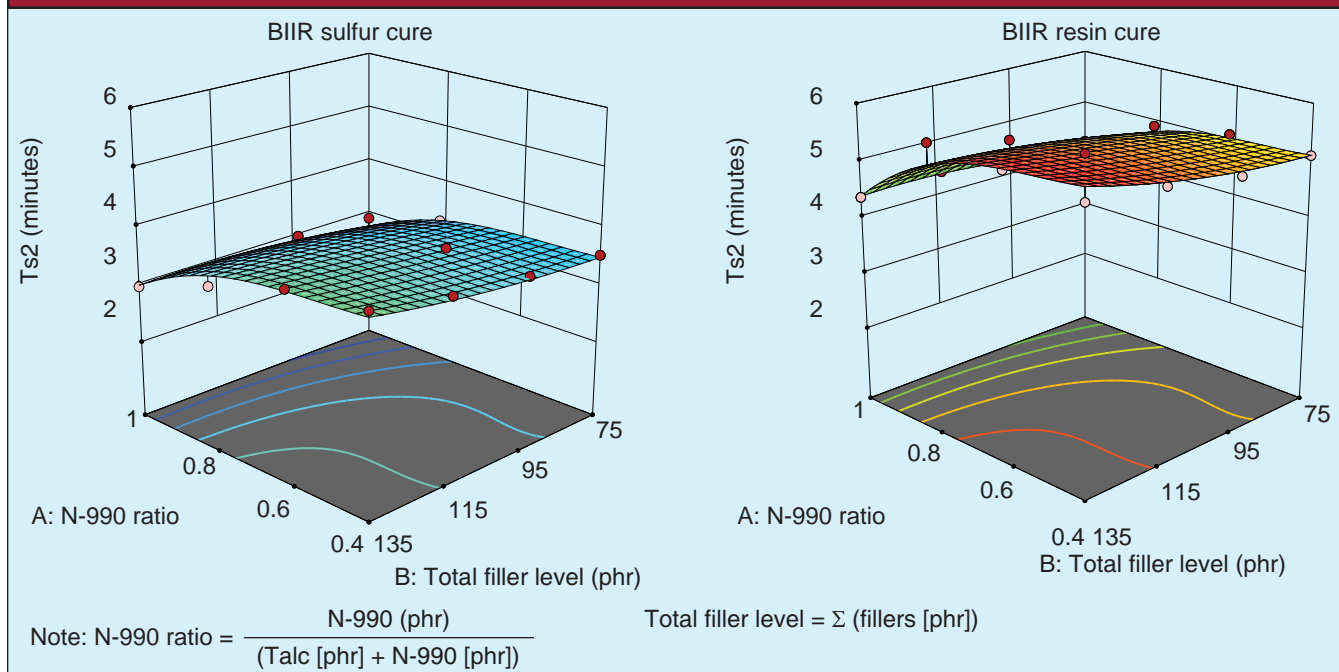
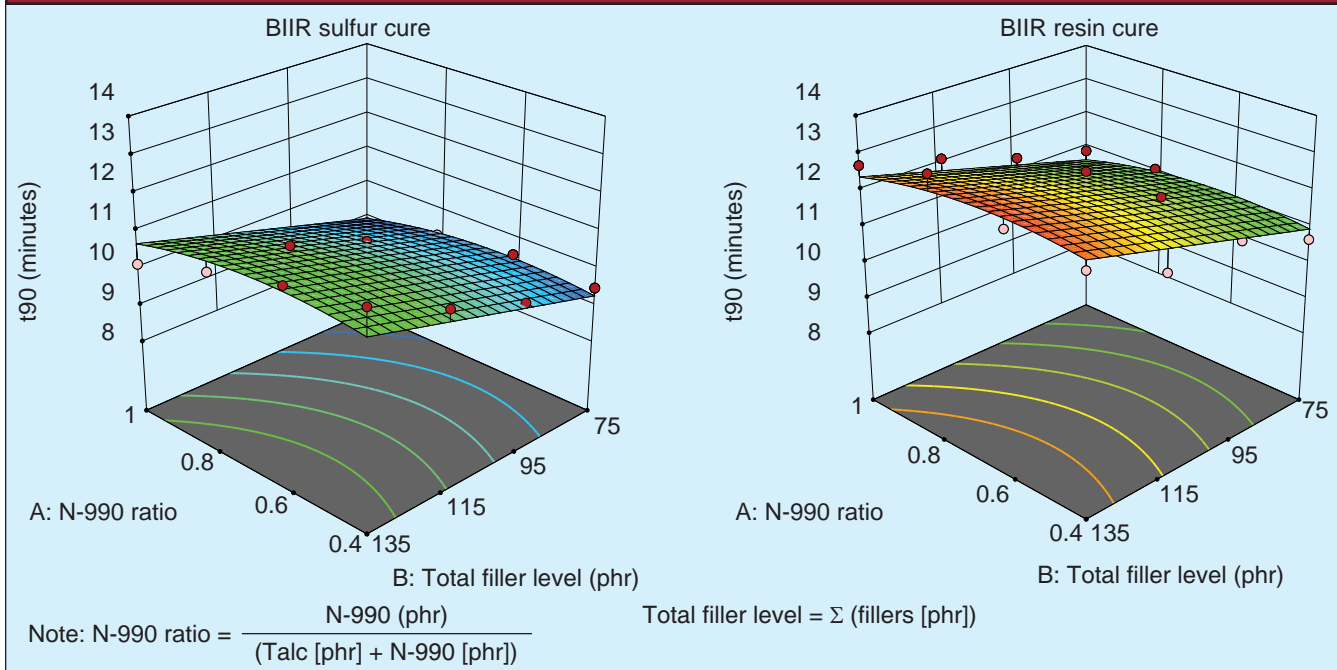


Figure 13 - Tc90 cure time response surface models for compounds, MDR at 1° arc and 160°C (ASTM D5289)



decrease in Mooney viscosity. It is important to remember that the Mooney viscometer is a low shear rate instrument, and results may not correlate well to higher shear rate processes.

Figure 10 displays the response surface models for storage modulus, G' , at 1.0% strain amplitude, 0.1 Hz and 60°C. Values of storage modulus ranged from 550 to 1,000 kPa.

The storage modulus (G') tends to increase slightly with the

N-990 ratio, and strongly with total filler loading. The large increase in small amplitude storage modulus with increasing total filler loading agrees with the long established theory originally proposed by Payne (ref. 10). The storage modulus is minimized at 75 phr total filler loading and maximized at 135 phr total filler loading. Again, this effect can be considered complex in that the oil content varied to achieve iso-hardness. The oil con-

Figure 14 - durometer A hardness response surface models of compounds tested at 23°C (ASTM D2240)

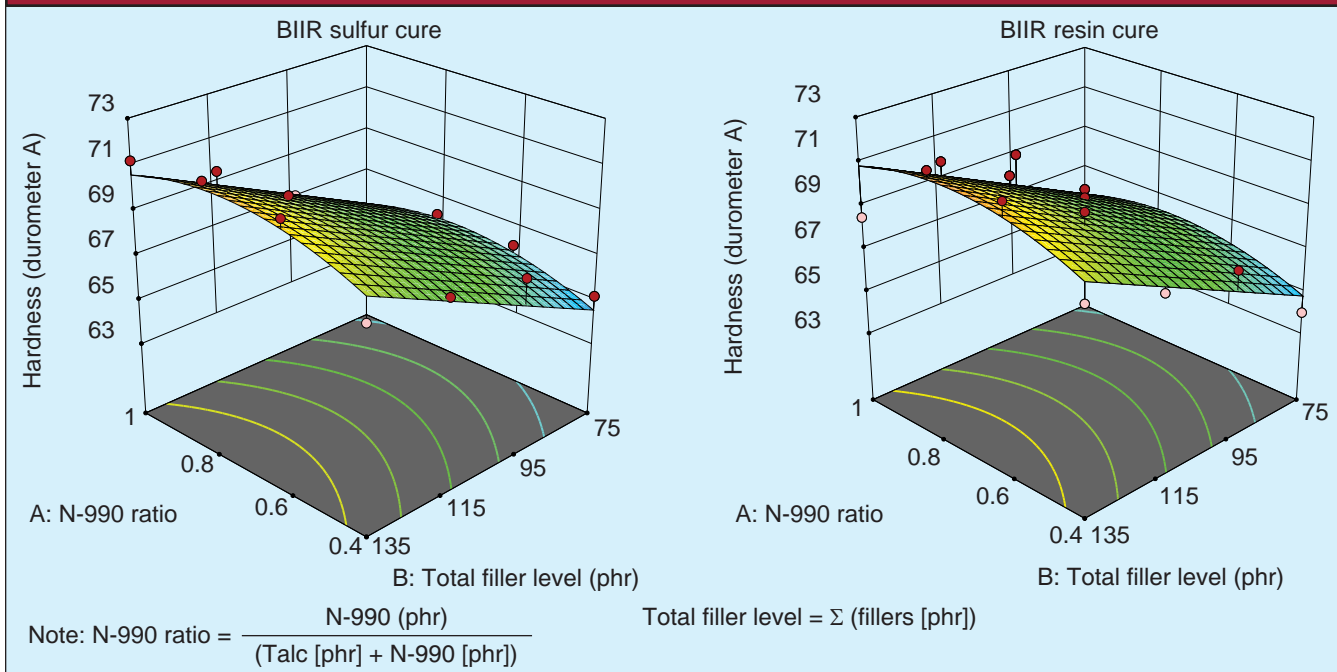
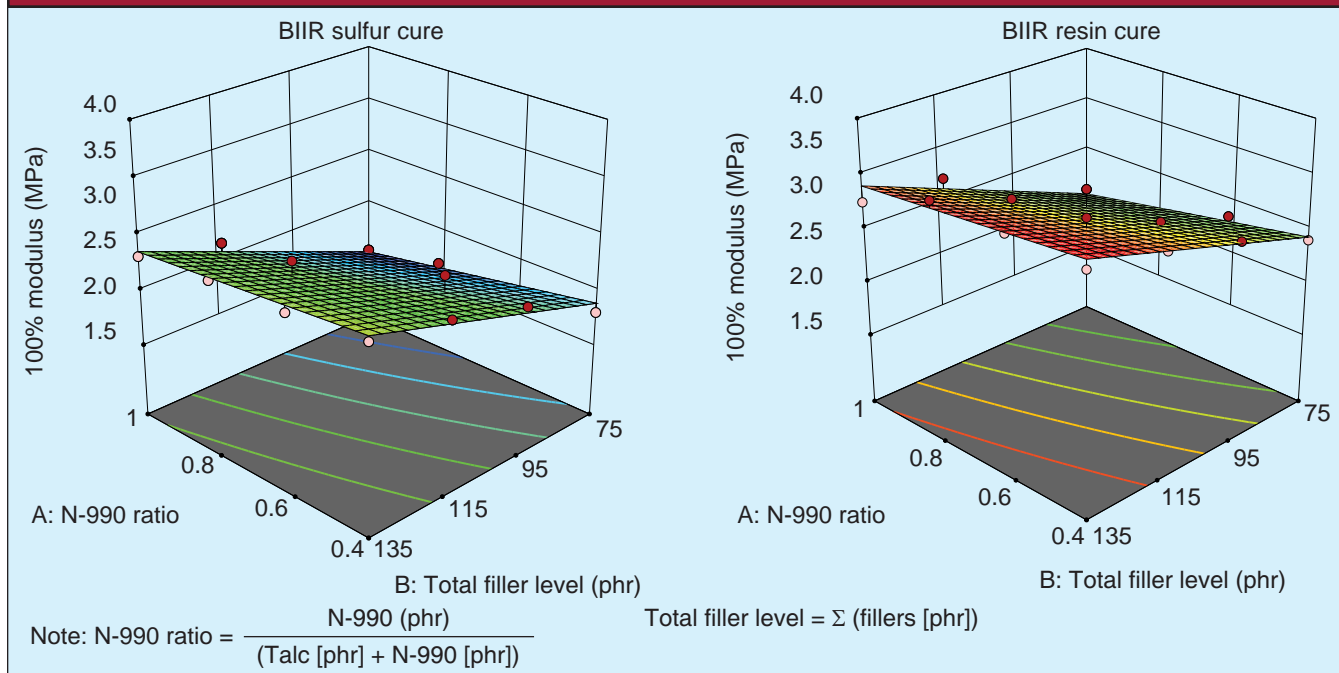


Figure 15 - 100% modulus response surface models for compounds tested at 23°C (ASTM D412)



tent generally increased with filler loading, and that is a major contributor to the decrease in storage modulus.

Figure 11 shows the response surface models for $\tan \delta$ at 0.5 Hz and 100°C. Values of $\tan \delta$ ranged from 0.58 to 0.82, and tended to increase with increasing total filler loading and decreasing N-990 ratio. Values were a maximum at an N-990 ratio of 0.4 and total filler loading of 135 phr.

Figure 12 shows the response surface models for scorch time, ts_2 , 1° arc and 160°C. The sulfur cure system had scorch times

between 2.9 and 4.0 minutes, while the resin cure system had scorch times between 3.7 and 5.6 minutes. The lowest scorch times at any given total filler loading were found at an N-990 ratio of 1.0. Maximum scorch times were generally found at higher total filler loadings and N-990 ratios of 0.6 and 0.8.

Figure 13 displays the response surface models for cure time, Tc_{90} , at 1° arc and 160°C. The sulfur cure system had cure times between 8.8 and 11.8 minutes, while the resin cure system had cure times between 10.6 and 13.2 minutes. Cure times increased

Figure 16 - 200% modulus response surface models for compounds tested at 23°C (ASTM D412)

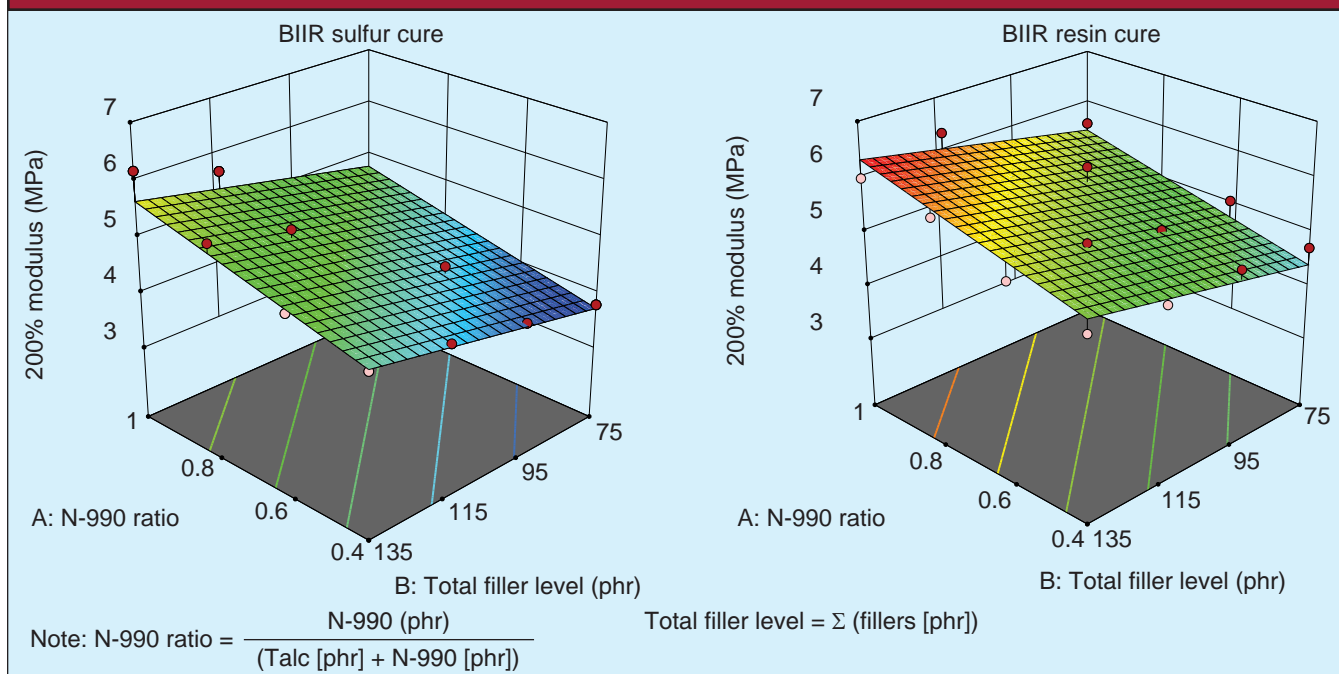
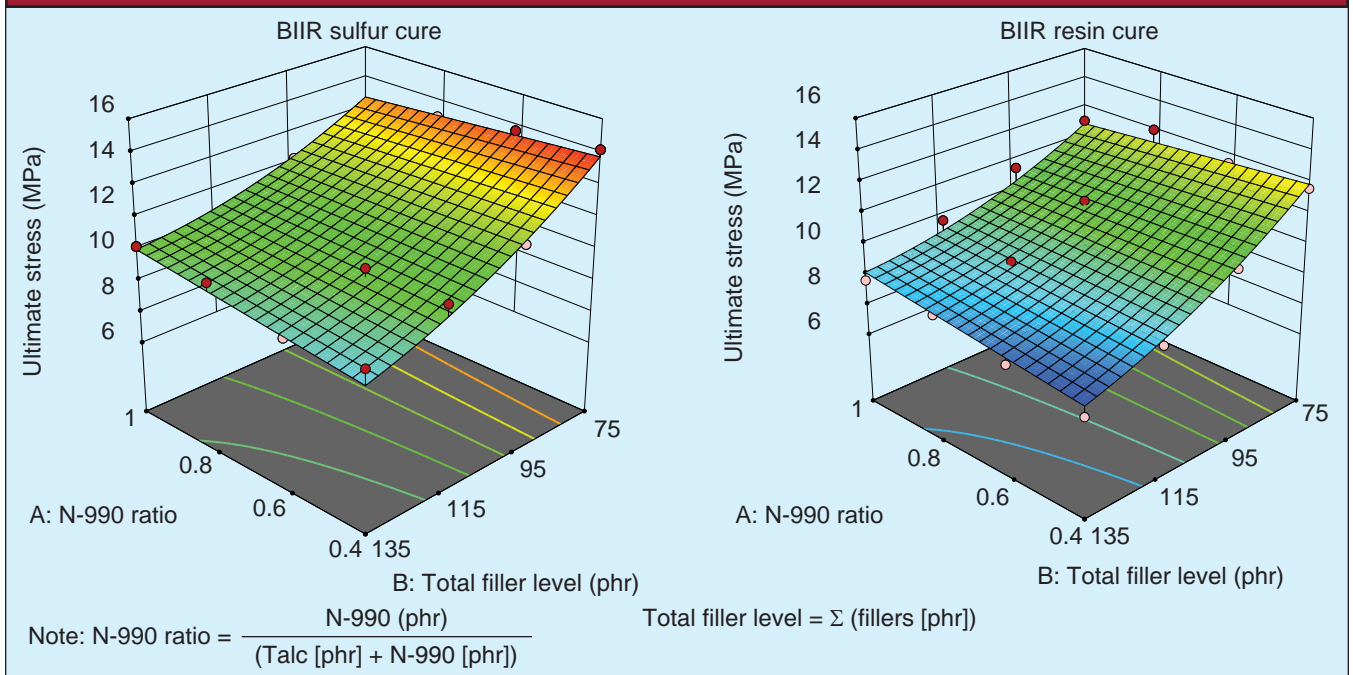


Figure 17 - ultimate stress/tensile strength response surface models for compounds tested at 23°C (ASTM D412)



with increasing total filler loading. Cure times were minimized for the sulfur cure system at an N-990 ratio of 1.0 and total filler loading of 75 phr. Cure times were minimized for the resin cure system at a total filler loading of 75 phr with no significant effect from the N-990 ratio. Shorter cure times allow for shorter mold cycle times and potentially higher productivity. The cure system can be adjusted depending on the balance of scorch time, cure

time and physical properties required.

Physical properties

Physical properties were measured using ASTM slabs and buttons cured at 160°C. The physical property requirements are dependent on end use demands. As an example, a hose liner may need higher tensile and modulus, whereas a seal may need

Figure 18 - elongation at break response surface models for compounds tested at 23°C (ASTM D412)

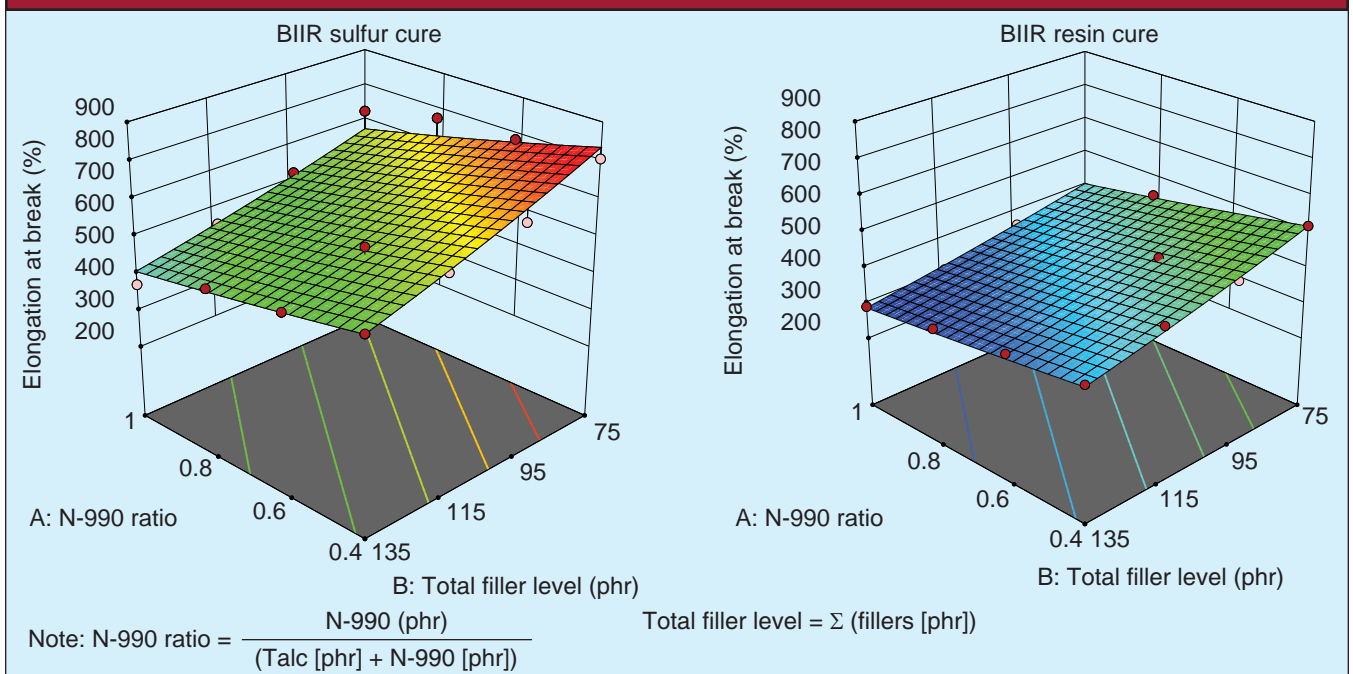
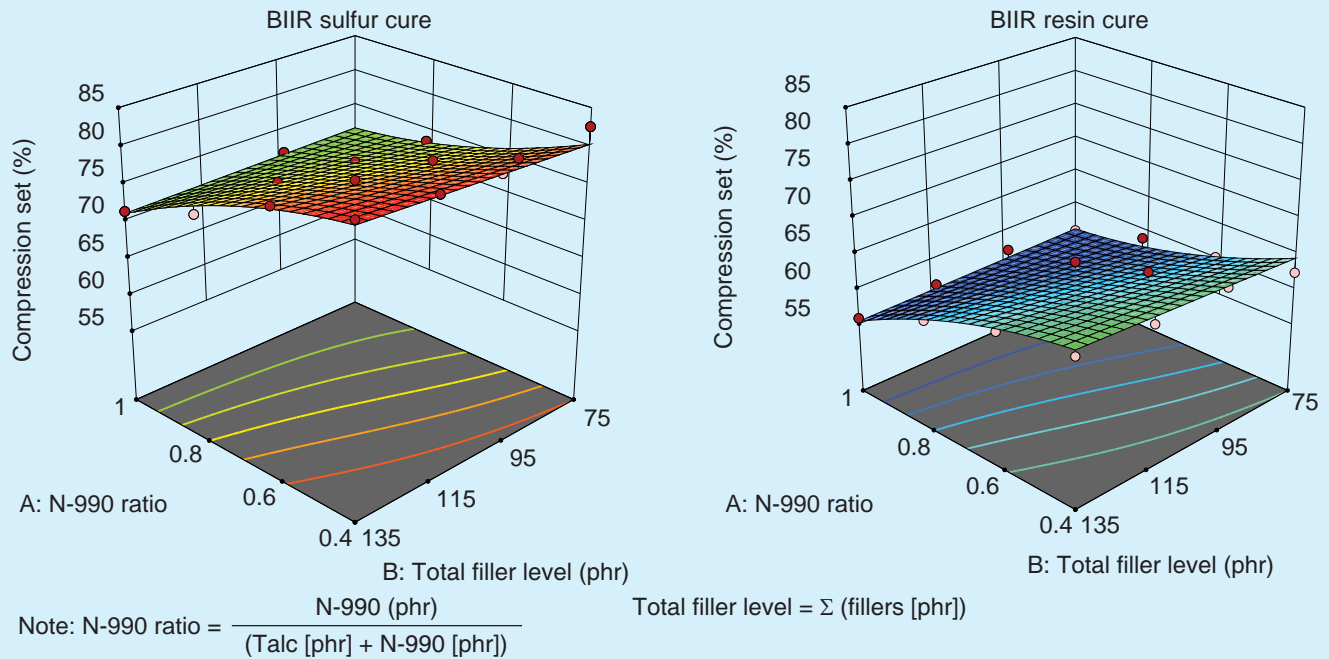


Figure 19 - compression set response surface models for compounds tested at 25% deflection, 100°C, 70 hours tested at 23°C (ASTM D395)



lower compression set. Therefore, the intention of the optimal properties may suit one application, and yet a different formulation variant may suit a different application.

Figure 14 shows the response surface models for durometer A hardness. Hardness values ranged from 64 to 72 points. All compounds met iso-hardness constraint of 68 ± 5 . The hardness tended to increase with increasing total filler loading, despite the

use of additional free oil to compensate.

Figure 15 displays the response surface models for stress at 100% strain. Values ranged from 2 to 3.5 MPa, with the resin cure system having significantly higher stiffness. Modulus tended to increase with increasing total filler loading and decreasing N-990 ratio with maxima at 135 phr and 0.4. Figure 16 shows the response surface models for stress at 200% strain.

Figure 20 - oxygen permeation response surface models for compounds tested at 40°C, 1 atm (ASTM D1434)

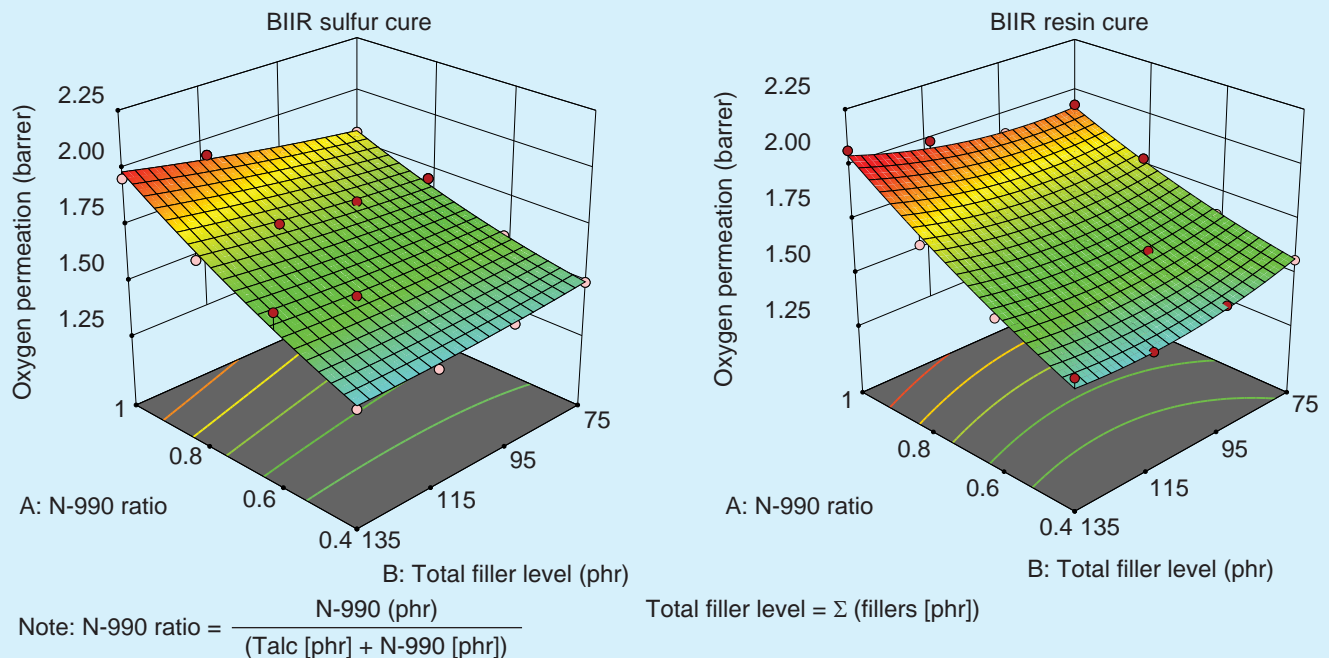
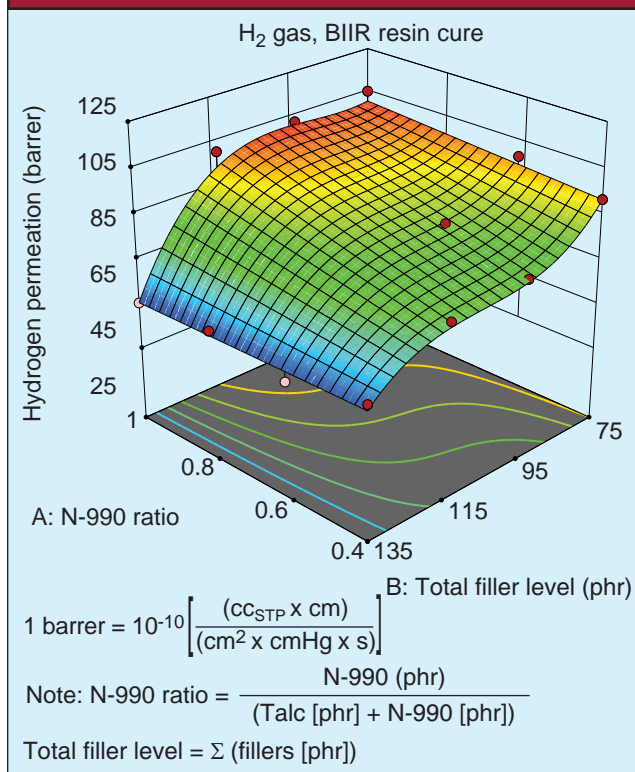


Figure 21 - H₂ gas permeation response surface models for BIIR-resin cured compounds tested at 90°C, 6.8 atm



Values ranged from 3.7 to 6.3 MPa. As opposed to the stress at 100% strain, stiffness increased with increasing total filler loading and increasing N-990 ratio with maxima at 135 phr and 1.0.

Figure 17 displays the response surface models for tensile strength. Values ranged from 8.4 to 12.1 MPa for the sulfur cure system, and 6.9 to 11.0 MPa for the resin cure system. Tensile strength decreased significantly as total filler loading was increased. For applications requiring higher tensile strength around 10.5 MPa (~1,500 psi), such as pressurized hose, a lower total filler loading should be used. For applications requiring only moderate tensile strength around 7 MPa (~1,000 psi), such as seals, all filler loading levels produced adequate results.

Figure 18 shows the response surface models for elongation at break. Values ranged from 370% to 710% for the sulfur cure system, and 290% to 520% for the resin cure system. Elongation decreased strongly with increasing total filler loading and N-990 ratio. To maximize elongation, a total filler loading of 75 phr and an N-990 ratio of 0.4 should be used.

Figure 19 shows the response surface models for compression set measured after 70 hours at 100°C. Values ranged from 69% to 83% for the sulfur cure system, and 55% to 66% for the resin cure system. Compression set decreased significantly as N-990 ratio increased, and increased slightly as the total filler loading increased. For sealing applications where compression set is critical, the resin cure system and high N-990 ratios will provide the best results. The compression set of the sulfur cure system at low N-990 ratios was above 80%, and would be less suitable for static sealing applications.

Permeation results

In figure 20, the O₂ permeation data show a strong correlation with filler loading and N-990 ratio, with lower N-990 ratios and higher filler loadings providing a minimum permeation value for both the resin and sulfur cured compounds. The resin cured samples tend to have a slightly lower permeation rate overall. This may be due in part to the thermoplastic nature of the curative package, minor differences in the final cure state (crosslink density, with higher cure density leading to reduced chain mobility) or even caused by changes in the filler distribution within the compound itself. Additional study would be required to better understand this difference.

Hydrogen permeation was measured only for the resin cured X_Butyl compound series (BIIR resin), and the results are shown in figure 21. The predicted response surface model shows the higher filler loading. Unlike O₂ gas, the permeation resistance for H₂ gas is independent of the Mistrion HAR talc loading in the compound. In fact, at an N-990 ratio of 1 (no HAR talc filler in the compound), the permeation resistance closely compares to compounds with an N-990 ratio of 0.4 (highest HAR loading). This is good evidence that the Thermax N-990 has a unique effect on the permeation resistance of H₂, and not O₂ gas. At constant filler loadings, the permeation resistance is similar for all N-990 ratios. The response surface model for hydrogen gas permeation shows a complexity in response that builds inference as to the graphitic nature of Thermax N-990 causing increased tortured path resistance.

Based on the models generated from the analysis of the compounds in this design space, it is possible to predict the optimal formulations for a seal and a hose compound by applying the appropriate weighting for the most desirable traits.

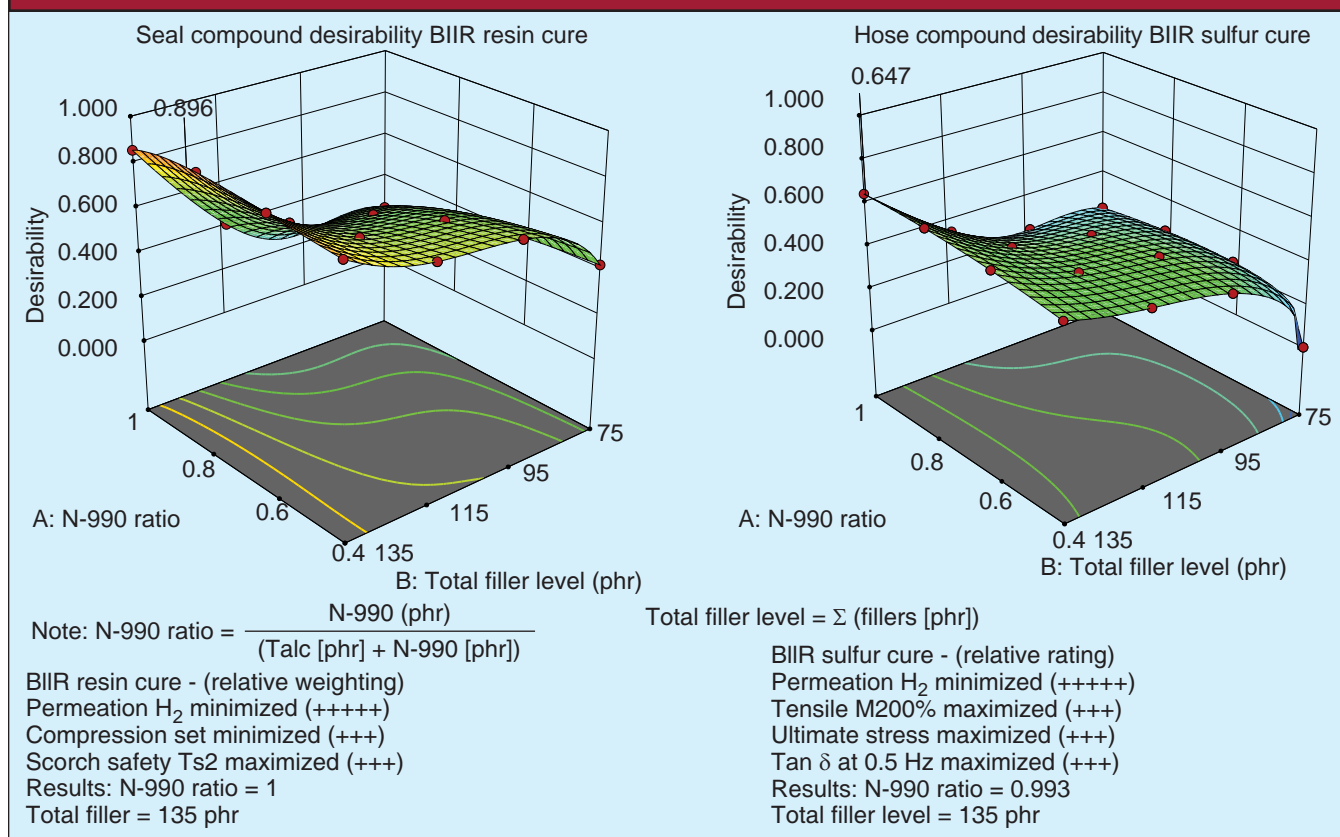
For seal applications, in order to maintain a good H₂ gas barrier, a rubber gasket or o-ring must have a lowest possible H₂ permeation and low compression set value, while at the same time maximizing scorch safety to provide the necessary processing window for seal manufacturing. From the compounds evaluated in this study, the optimum formulations for seals are shown in figure 22 (left), where resin cured compounds with high filler loading (135 phr total, with 105 phr N-990, 30 phr N-330 and with no HAR talc) provided the best overall performance.

For fabrication of hoses, the final compression set becomes less significant; and the processing and cure system more compatible with continuous vulcanization processes is preferred. The ideal compound will have the lowest possible H₂ permeation, highest tensile (M200) and ultimate stress values; and in general, a higher tan δ value is preferred for extrusion processes. From the set of compounds studied here, the most desirable compound compositions are shown in figure 22 (right), where sulfur cured compounds, once again with high filler loading (135 phr total, with 105 phr N-990, 30 phr N-330 and with no HAR talc) compound, provided the best overall performance.

Conclusions

Hydrogen permeation resistance of X_Butyl BB 2030 using a filler system with Thermax N-990, N-330 and Mistrion HAR talc with both a sulfur and a resin cure system were studied in

Figure 22 - predicted compound desirability models for an H₂ seal compound (resin cured compound) and an H₂ hose compound (sulfur cured compound)



this report. This work brings valuable insight for the design of optimized delivery and on-board storage and transport systems for hydrogen gas. The study addresses application concerns with low loss hydrogen sealing for flexible hoses and seals that work to 7 atmospheres of pressure and 90°C, and brings attention to design engineering needs.

Careful selection of the elastomer and filler system can achieve low permeation rates. X_Butyl BB 2030 was chosen due to the unique permeation resistance properties compared to other elastomers. By studying ratios of Thermax N-990 and total filler loading, it is possible to reduce the permeation rates of hydrogen gas in X_Butyl by a factor of 60%. Typically, such dramatic changes in permeation resistance for elastomeric composites requires high aspect ratio fillers, such as Mistrion HAR talc, as found for the O₂ permeation testing in this study and in the literature. This trend was not found in the case of H₂ gas, for which lower permeation rates can be achieved with Thermax N-990 alone; and is relatively independent of the loading of Mistrion HAR talc in the system. Based on the compounds studied in this article, it was possible to predict starting formulations for optimum H₂ permeation resistant seals (resin cure) and hoses (sulfur cure) using an N-990/N-330 filler system, which in fact does not contain HAR talc.

Additional work will be undertaken to better understand the utility of this Thermax N-990 filler system for hydrogen permeation resistant compounds. The effect of temperature on the permeation resistance in these compounds, as well as additional in-

sights into the mechanism of the increased permeation resistance for hydrogen gas compared to other gases, will be explored.

This article is based on a paper presented at the 196th Technical Meeting of the Rubber Division, ACS, October 2019.

References

1. Toyota Mirai Fuel Cell Vehicle, photo from Toyota's website.
2. M.W. Fitch, et al., "Permeation of several gases through elastomers, with emphasis on the Deuterium/hydrogen pair," Department of Chemical Engineering, University of Texas at Austin, and Group WX-5, Los Alamos National Laboratories, Los Alamos (1992).
3. T. Graham, Phil. Trans. Roy. Soc. (London), 156, 399, (1866).
4. S. Von Wroblewski, Ann. Phys., 8, 29 (1879).
5. G.J. Van Amerongen, Rubber Chem. Tech., 37, 1,065 (1964).
6. S.C. George and S. Thomas, Prog. Polym. Sci. 26 (2001), pp. 985-1,017.
7. C.R. Herd, "Morphology and surface properties," presented at the ACS Meeting, May 1996.
8. J. Petucci, et al., "Diffusion, adsorption and desorption of molecular hydrogen on graphene and graphite," J. Chem. Phys. 139, 044706 (2013).
9. A. Jelea, et al., Carbon 42, pp. 3,189-3,198, "Quantum study of hydrogen-oxygen-graphite interactions," Elsevier Ltd. (2004).
10. A.R. Payne, "The dynamic properties of carbon black-loaded natural rubber vulcanizates, part 1," J. Appl. Polym. Sci. 6 (19), pp 57-5 (1962).